Hong Kong J Radiol. 2025;28(2):e128-40. Published 13 June 2025 | https://doi.org/10.12809/hkjr2417879

PICTORIAL ESSAY

Clinical Applications of Amino Acid Positron Emission Tomography–Magnetic Resonance Imaging in Neuro-Oncology: A Pictorial Essay

JCY Lam[1], SSM Lo[2], DYW Siu[2], PW Cheng[2]

[1]Department of Radiology, Tuen Mun Hospital Neuroscience Centre, Hong Kong SAR, China
[2]Scanning Department, St Teresa's Hospital, Hong Kong SAR, China

INTRODUCTION

Management of an intracranial neoplasm involves sophisticated neuroimaging investigations. Magnetic resonance imaging (MRI) is important in diagnosing primary brain tumour, though it has limitations. Gadolinium-enhanced MRI can assess the morphology but does not allow determination of tumour metabolism. It also has limitations in evaluating non-enhancing gliomas. Magnetic resonance spectroscopy (MRS) provides information on the presence of neuronal and membrane metabolites. However, it has poor spatial resolution and is prone to susceptibility artefact. ^{18}F-fluorodeoxyglucose positron emission tomography (PET)/computed tomography can give clues on tumour metabolism, yet interpretation can be unreliable due to high background brain uptake of ^{18}F-fluorodeoxyglucose. In past decades, metabolic imaging with amino acid tracers (e.g., ^{11}C-methionine [^{11}C-MET] and ^{18}F-fluoroethyl-L-tyrosine [^{18}F-FET]) has established its added value in the non-invasive investigation of brain tumours. The pairing of amino acid PET (AA-PET) with MRI allows evaluation of both tumour morphology and corresponding metabolic activity in a single visit to the imaging institution. This pictorial review will illustrate the clinical applications of AA-PET/MRI in neuro-oncology.

MECHANISM OF RADIOLABELLED AMINO ACID POSITRON EMISSION TOMOGRAPHY TRACER

Amino acids play an essential role in many cellular processes. In addition to passive diffusion, the majority of amino acid uptake is governed by carriers such as large amino acid transporters (LATs) and the alanine-serine-

Correspondence: *Dr JCY Lam, Department of Radiology, Tuen Mun Hospital Neuroscience Centre, Hong Kong SAR, China*
Email: ljc057@ha.org.hk

Submitted: 24 July 2024; Accepted: 9 October 2024.

Contributors: All authors designed the study, acquired the data, analysed the data, drafted the manuscript, and critically revised the manuscript for important intellectual content. All authors had full access to the data, contributed to the study, approved the final version for publication, and take responsibility for its accuracy and integrity.

Conflicts of Interest: All authors have disclosed no conflicts of interest.

Funding/Support: This study received no specific grant from any funding agency in the public, commercial, or not-for-profit sectors.

Data Availability: All data generated or analysed during the present study are available from the corresponding author on reasonable request.

Ethics Approval: This study was approved by St Teresa's Hospital Research Ethics Committee, Hong Kong (Ref No.: MGT-POL-008). The patients were treated in accordance with the Declaration of Helsinki. Informed consent was obtained from patients aged 18 years or older and the carers of patients aged under 18 years for all treatments and procedures, as well as for the publication of this article and the accompanying images.

Acknowledgement: The authors thank the research staff at the Scanning Department of St Teresa's Hospital for their assistance in data collection.

cysteine transporter (ASCT). An LAT subtype, LAT1, is present at both the luminal and abluminal sides of the endothelial cell; it plays a crucial role in transporting amino acids across the blood-brain barrier. Unlike gadolinium contrast used in MRI, an intact blood-brain barrier does not limit the uptake of amino acids into an actively proliferating neoplasm.

Compared with healthy brain tissue, brain tumour cells significantly overexpress LAT1 and ASCT2, a subtype of ASCT, resulting in increased amino acid uptake by tumour and increased amino acid metabolism. Normal brain tissue has low expression of these transporters, resulting in the markedly lower amino acid tracer background activity and high tumour-to-normal tissue contrast in AA-PET.

An increased rate of metabolism in biological processes involving deoxyribonucleic acid and protein synthesis for cell growth and proliferation results in increased uptake of methionine, which involves LAT1, ASCT and ASCT2 transporters. The major limitation of ^{11}C-MET PET study is the short half-life of the ^{11}C-radiotracer (20 minutes). An on-site cyclotron facility is required for its production prior to the study.

^{18}F-FET, another amino acid tracer, shows similar uptake and image contrast by brain tumours compared with ^{11}C-MET. ^{18}F-FET is metabolically inert which facilitates kinetic analysis for distinguishing high-grade from low-grade gliomas. It is easier to produce and has a longer half-life (110 minutes), making it more convenient for clinical applications.

DIFFERENTIATING NEOPLASMS AND NON-NEOPLASTIC LESIONS

^{11}C-MET PET imaging and ^{18}F-FET PET imaging can be used to distinguish gliomas from non-neoplastic lesions. Early diagnosis can guide timely treatment and avoid unnecessarily invasive workups, particularly for paediatric patients and for lesions in eloquent areas.

Based on the 2019 European guidelines,[1] qualitative and semi-quantitative evaluations can be performed with cutoff thresholds depending on clinical questions. To differentiate neoplastic from non-neoplastic tissue, the recommended cutoff thresholds for definition of biological tumour volume are: (1) a standardised uptake value (SUV) of ^{11}C-MET PET imaging >1.3 × the mean value of healthy brain[2]; or (2) a SUV of ^{18}F-FET PET imaging >1.6 to 1.8 × the mean value of healthy brain.[3] For ^{18}F-FET PET imaging, the recommended threshold to differentiate between neoplastic and non-neoplastic tissue is a maximum tumour-to-background ratio (TBR) [TBR_{max}] of 2.5 or a mean TBR (TBR_{mean}) of 1.9.[1] High tracer uptake with TBR_{max} exceeding 2.5 was found to have a high positive predictive value for detecting neoplastic lesions.[4] A commonly used threshold for ^{11}C-MET uptake is a TBR_{max} of 1.3 to 1.5.[2,5]

A 15-year-old patient presented with panhypopituitarism. MRI of the pituitary gland before and after gadolinium contrast showed pituitary stalk thickening with a hypoenhancing lesion involving the pituitary gland and stalk (Figure 1). ^{11}C-MET PET/MRI showed strong tracer activity within the gland and along the stalk, suggesting an active neoplastic process (Figure 2). The diagnosis

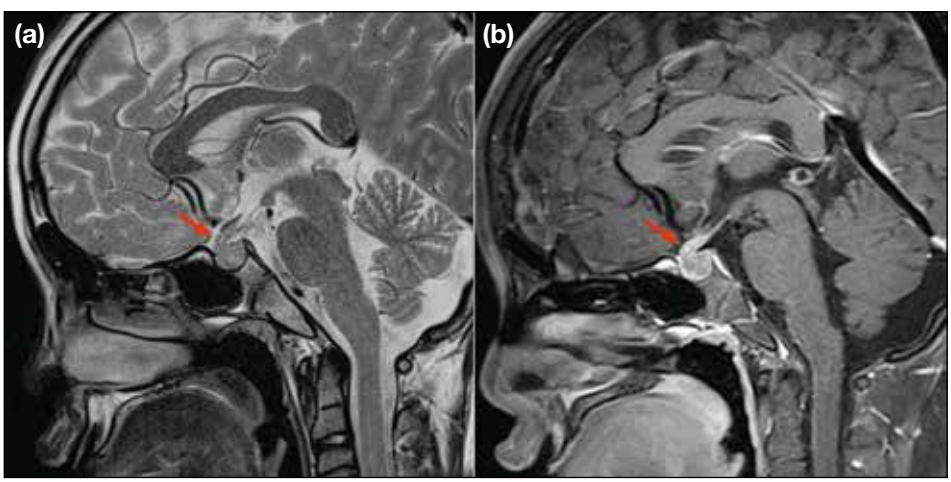

Figure 1. Pituitary gland germinoma of a 15-year-old patient. (a) Pituitary stalk thickening with prominent size of the pituitary gland is seen on T2-weighted sagittal magnetic resonance imaging (MRI) [arrow]. (b) Hypoenhancing lesion involves the pituitary gland and stalk on post-gadolinium T1-weighted MRI [arrow].

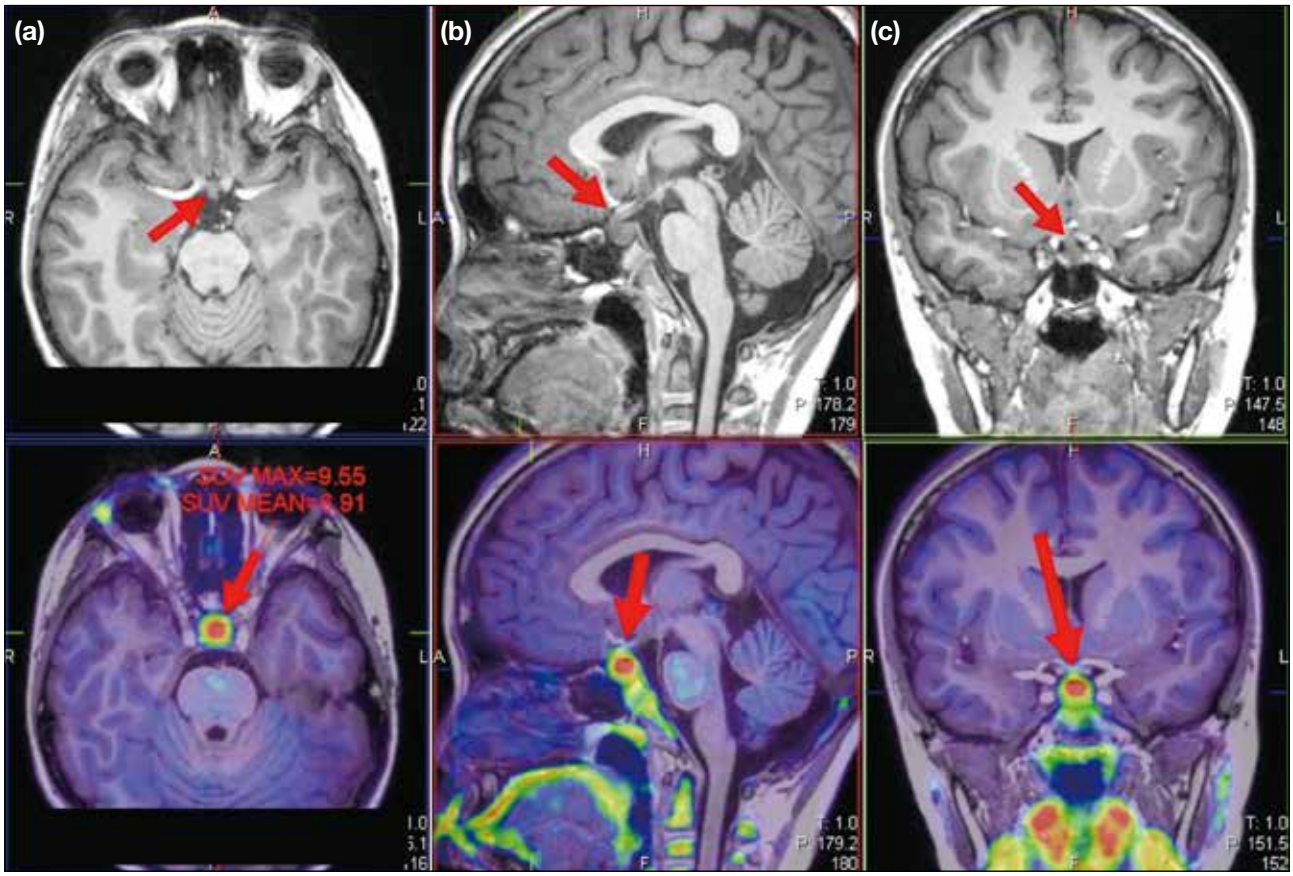

Figure 2. Pituitary gland germinoma of the same patient in Figure 1. Pituitary stalk thickening with prominent pituitary gland is seen on pre-treatment T2-weighted magnetic resonance images (upper row) [arrows]. Strong ^{11}C-methionine tracer uptake is noted within the pituitary gland and along the pituitary stalk on pre-treatment hybrid positron emission tomography–magnetic resonance images (lower row) [arrows]. (a) Axial view. (b) Sagittal view. (c) Coronal view.
Abbreviations: SUV MAX = maximum standardised uptake value; SUV MEAN = mean standardised uptake value.

was biopsy-proven pituitary gland germinoma. The patient underwent chemoradiation. Follow-up ^{11}C-MET PET/MRI at 3 and 6 months showed normalisation of tracer uptake in the pituitary gland (Figure 3), suggesting complete response to treatment.

A 12-year-old patient presented with left-sided weakness. Computed tomography of the brain showed a hyperdense lesion in the right basal ganglia. MRI showed an ill-defined T2-weighted hyperintense lesion in the right posterior basal ganglia and the thalamus with enhancement and restricted diffusion. No choline peak was detected on MRS (Figure 4). ^{11}C-MET PET/MRI showed significantly increased ^{11}C-MET tracer activity (TBR_{mean} = 1.80; TBR_{max} = 2.24) [Figure 5], suggesting an active neoplastic process. The patient was treated with chemoradiation. Follow-up PET/MRI showed decreasing T2-weighted signal and no residual ^{11}C-MET tracer activity in the right basal ganglia and the thalamus (Figures 6 and 7), suggesting complete response to treatment. For lesions in eloquent areas, AA-PET can depict the location of highest metabolic activity to indicate the most appropriate site for biopsy and increase the chance of obtaining the best representative tumour tissue. AA-PET also has advantages in detecting foci of high-grade glioma within a background of lower-grade tumour,[6] particularly when conventional MRI fails to identify heterogeneity.

With good tumour-to-background signal contrast, AA-PET/MRI can also be performed for spinal tumours. A 50-year-old patient presented with limb weakness and numbness. MRI of the cervical spine showed syringohydromyelia with an enhancing soft tissue nodule at the C6 to C7 vertebrae (Figure 8). ^{18}F-FET PET/MRI showed increased tracer uptake at the corresponding

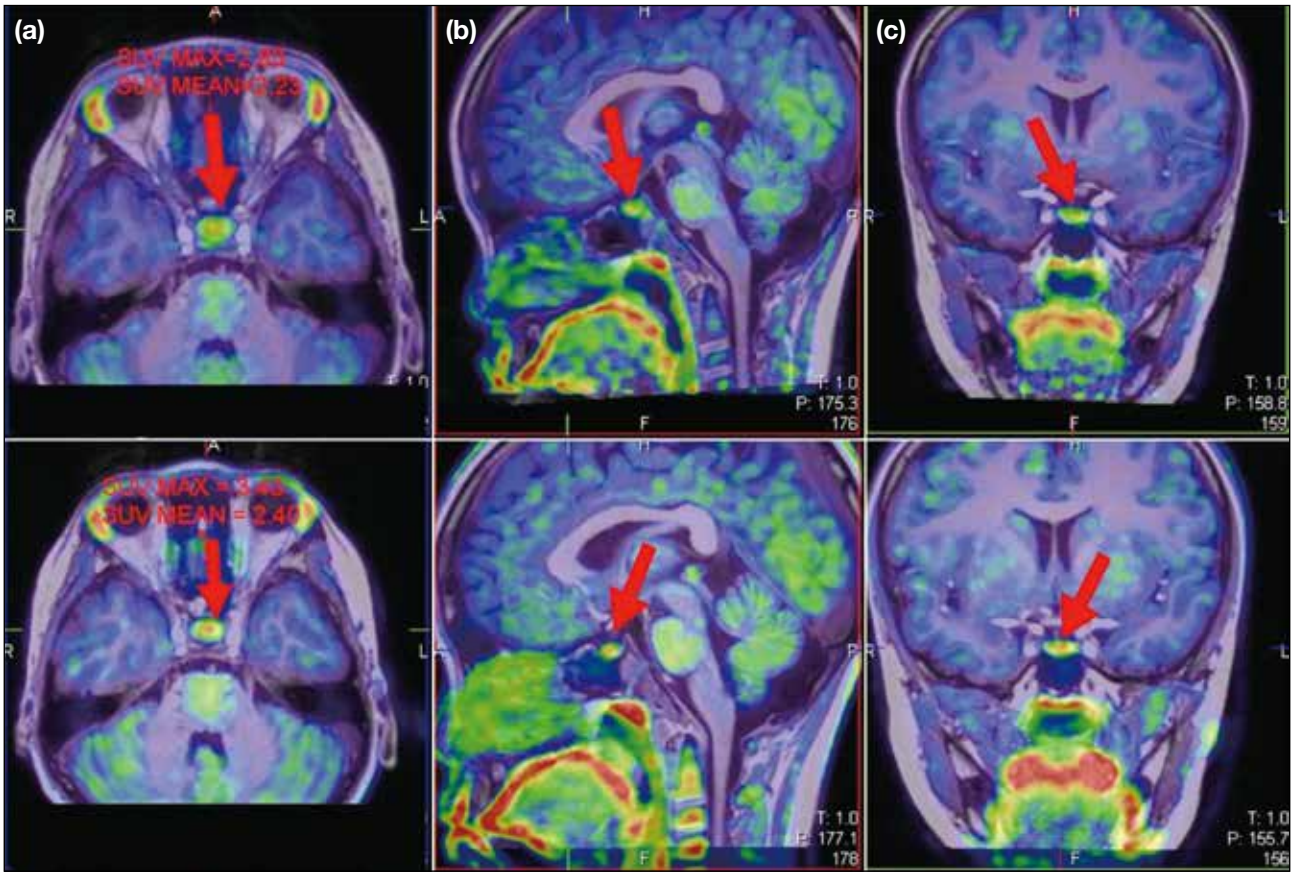

Figure 3. Pituitary gland germinoma of the same patient in Figure 1. Normalisation of tracer uptake in the pituitary gland (arrows) is seen on 3-month (upper row) and 6-month (lower row) follow-up ^{11}C-methionine positron emission tomography. (a) Axial view. (b) Sagittal view. (c) Coronal view.
Abbreviations: SUV MAX = maximum standardised uptake value; SUV MEAN = mean standardised uptake value.

site of enhancing soft tissue nodule with significantly increased TBR_{mean} of 2.02 and TBR_{max} of 3.38 (Figure 9), suggesting active neoplastic growth. The wall of the syrinx showed no increased tracer activity to suggest tumoural involvement. An AA-PET/MRI study in this case depicted the exact tumour site for operation. A study showed incorporation of AA-PET imaging increased the number of complete resections, which was associated with prolonged survival.[7]

TUMOUR GRADING AND PERIOPERATIVE APPLICATIONS

A study has shown that patients with high-grade gliomas exhibit significantly higher ^{18}F-FET tracer uptake than patients with low-grade gliomas.[4] In addition, the diagnostic performance for grading with ^{18}F-FET PET/MRI can be improved, given that high-grade tumours frequently show characteristic dynamic data with an early time to peak (TTP) within the first 10 to 20 minutes followed by a plateau or a descent of the time-activity curve.[8] Although a reliable differentiation of World Health Organization (WHO) grade III/IV and grade I/II gliomas is not possible because of a high proportion of active tumours among the latter, especially in oligodendrogliomas,[1] an early finding of low invasiveness of the tumour might help the neurooncologist decide on patient management. The recommended PET parameters[1] of ^{18}F-FET PET/MRI to differentiate WHO grade I/II versus grade III/IV glioma include a TBR_{max} of 2.5 to 2.7, a TBR_{mean} of 1.9 to 2.0, a TTP <35 minutes, or TAC pattern II (an early peak followed by a plateau) or III (a decreasing TAC).[1]

In 2021, the WHO classification of central nervous system tumours has incorporated molecular information into the diagnosis of brain tumours.[9] The grading system has been reformed and significantly restructured, especially for diffuse gliomas. The isocitrate

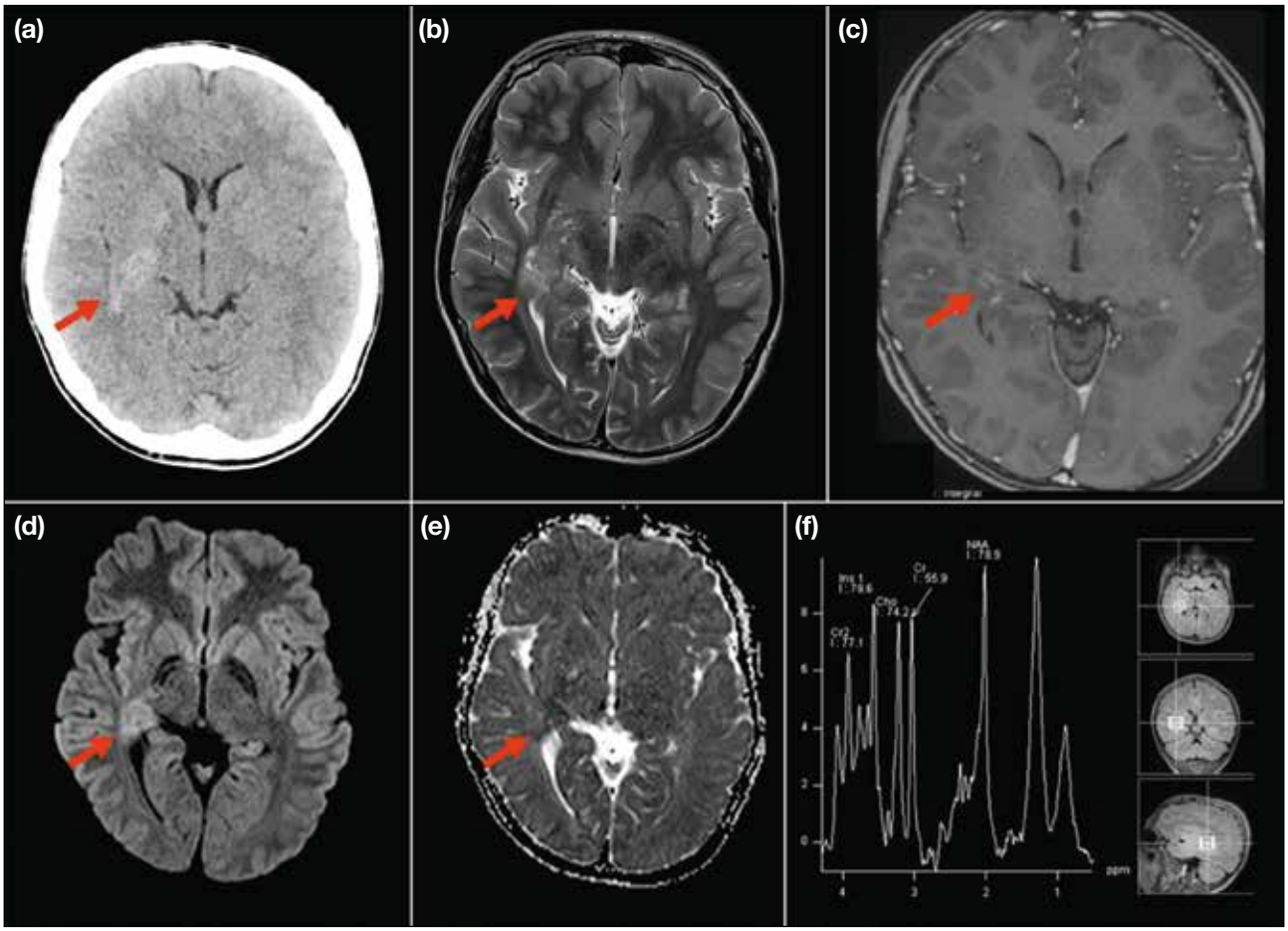

Figure 4. Basal ganglia germ cell tumour of a 12-year-old patient. (a) Hyperdense lesion on computed tomography (arrow). (b) Infiltrative T2-weighted hyperintense lesion in the right posterior basal ganglia and the thalamus (arrow) with mild enhancement on post-gadolinium T1-weighted magnetic resonance imaging (c) [arrow]. The corresponding lesion showed restricted diffusion on diffusion-weighted imaging (d) and apparent diffusion coefficient mapping (e) [arrows]. There is no significant elevation of choline peak on magnetic resonance spectroscopy (f).

dehydrogenase (IDH) mutation status has important diagnostic and therapeutic roles. Preoperative reliable prediction of IDH status can facilitate preliminary diagnosis of a high-grade tumour and prompt therapeutic strategies.

A reliable cutoff value for TBR_{max} or TBR_{mean} in conventional static ^{18}F-FET PET/MRI to differentiate IDH status is still under debate. A study with a large patient population showed a significantly shorter median TTP in IDH-wildtype gliomas compared with IDH-mutant gliomas.[10] Therefore, a short TTP in dynamic ^{18}F-FET PET/MRI serves as a good predictor of IDH-wildtype status, particularly in non–contrast-enhancing gliomas, with high diagnostic power.[10] Another study with smaller patient populations suggested combining TTP with TBR_{max} to achieve higher accuracies in predicting IDH mutation status.[11] Further studies are needed to verify the role of ^{18}F-FET PET/MRI in early detection of IDH status in glioma.

A 38-year-old patient presented with epilepsy. MRI of the brain showed a left temporal lobe infiltrative non-enhancing lesion with hyperintense T2-weighted signals (Figure 10). ^{18}F-FET PET/MRI showed a significant increase in tracer uptake (TBR_{mean} = 1.97) in the left temporal lobe (Figure 11), suggesting an active neoplastic process. Despite classical imaging features of a low-grade glioma in conventional MRI, a significant increase in tracer activity in ^{18}F-FET PET suggests a higher-grade lesion, which may alter clinical management.

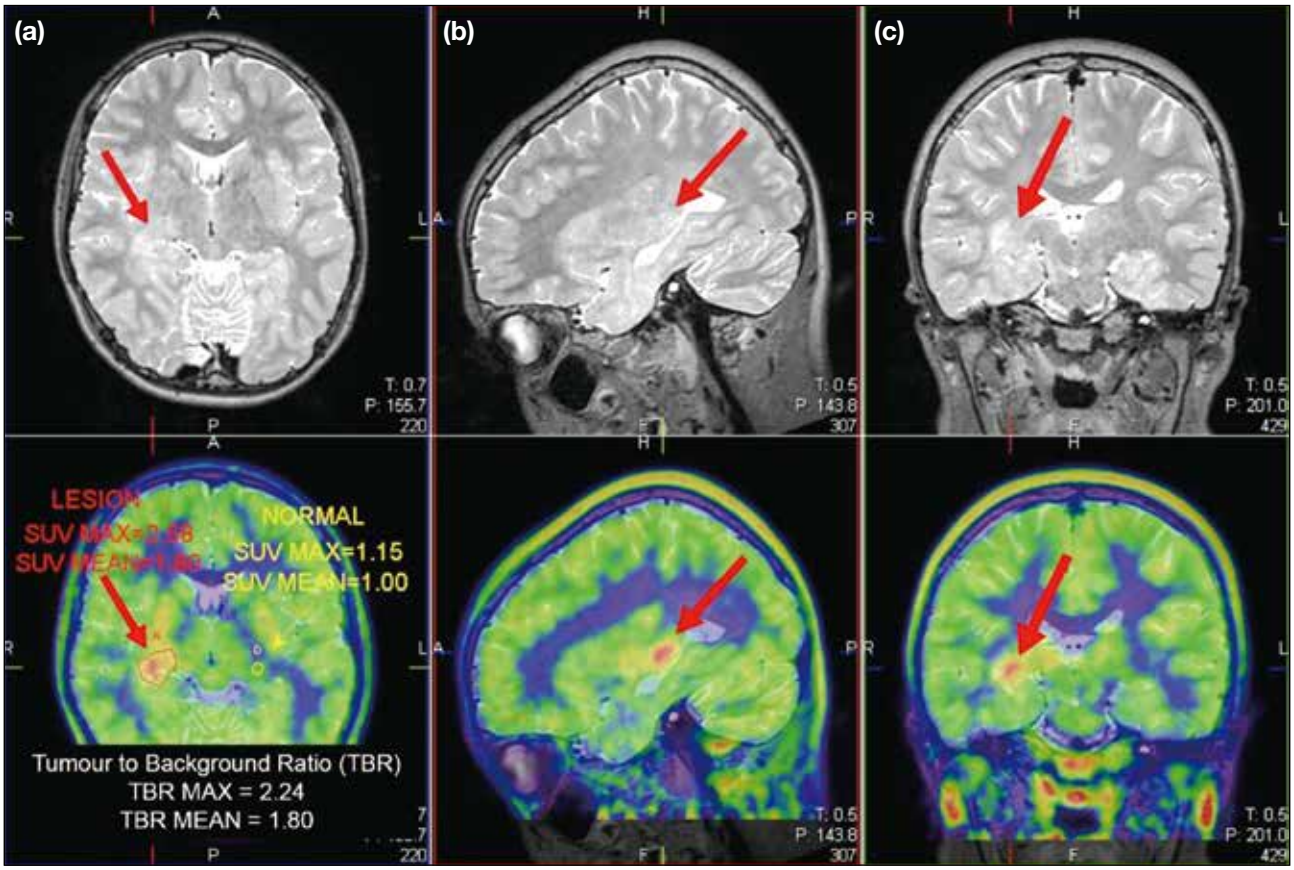

Figure 5. Basal ganglia germ cell tumour of the same patient in Figure 4, which is hyperintense in the right basal ganglia and the thalamus on T2-weighted magnetic resonance imaging (upper row) [arrows]. There is increased ^{11}C-methionine tracer activity in the right basal ganglia and the thalamus (lower row) [arrows]. (a) Axial view. (b) Sagittal view. (c) Coronal view.
Abbreviations: SUV MAX = maximum standardised uptake value; SUV MEAN = mean standardised uptake value; TBR MAX = maximum tumour-to-background ratio; TBR MEAN = mean tumour-to-background ratio.

TUMOUR TREATMENT RESPONSE ASSESSMENT AND DIFFERENTIATION FROM TREATMENT-RELATED PSEUDOPROGRESSION

Early detection of high-grade tumour recurrence can be achieved by performing AA-PET/MRI with follow-up MRIs, due to the high tumour-to-normal tissue contrast. A 63-year-old patient had a history of complete removal of a right temporal lobe glioblastoma (Figure 12). A follow-up MRI 9 months after surgery showed a new enhancing focus in the left frontal lobe subependymal region. ^{11}C-MET PET/MRI showed increased tracer uptake within the enhancing lesion, with a TBR_{mean} of 2.66 and a TBR_{max} of 2.49 (Figure 13), suggesting an active neoplastic process.

Conventional MRI has poor sensitivity and specificity in detecting post-therapy recurrence due to its limitations in differentiating between recurrence and radionecrosis. As viable tumour cells take up ^{18}F-FET more avidly than inflammatory cells, AA-PET offers advantages over conventional MRI, especially in haemorrhagic lesions.

A 53-year-old patient had a left cerebellopontine angle meningioma resected and irradiated. Follow-up MRI showed residual meningioma with postoperative changes (Figure 14). A new rim-enhancing lesion developed in the left cerebellum with central necrosis and internal haemorrhage (Figure 15). Advanced MRI techniques (i.e., MRI perfusion and MRS) did not provide useful information in the presence of haemorrhage. ^{18}F-FET PET/MRI showed significantly increased tracer uptake

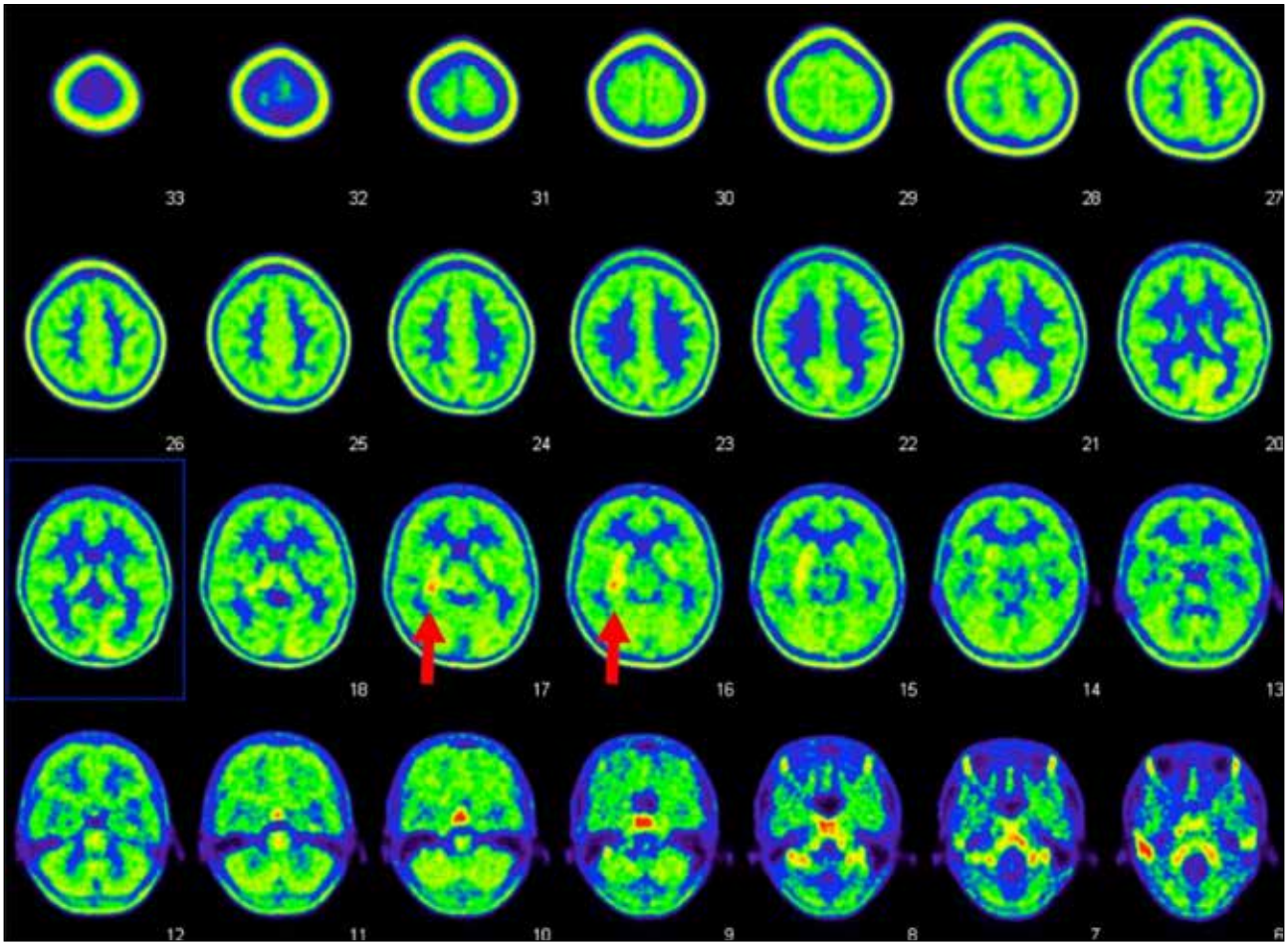

Figure 6. Basal ganglia germ cell tumour of the same patient in Figure 4. There is increased ^{11}C-methionine tracer activity in the right basal ganglia (arrows) in pre-treatment positron emission tomography.

along the enhancing wall of the lesion (TBR_{max} = 2.26; TBR_{mean} = 1.89) [Figure 16]. The commonly used thresholds to differentiate between true progression and pseudoprogression are a TBR_{max} of 2.3 for early pseudoprogression, and a TBR_{max} or a TBR_{mean} of 1.9 for late pseudoprogression.[1] Therefore, it suggested a high-grade active neoplastic process.

FALSE POSITIVITY OF AMINO ACID POSITRON EMISSION TOMOGRAPHY WITHOUT MAGNETIC RESONANCE IMAGING

Several physiological and pathological causes of increased amino acid tracer uptake have been reported, including cortical ischaemia,[12] sarcoidosis,[13] haematoma[14] and abscess.[15] Vascular lesions with amino acid tracer accumulation due to slow washout may also lead to misinterpretation.[16] Molecular PET, in combination with a multiparametric MRI, can provide both structural and functional information to reduce false positive cases that might be seen on AA-PET alone.

A 45-year-old patient presented with ataxia. MRI of the brain showed a heterogeneous T2-weighted hyperintense cortical right cerebellar lesion with perifocal vasogenic oedema. It showed intense solid enhancement without cystic component. ^{11}C-MET and ^{18}F-FET PET/MRI showed strong nodular tracer uptake in the corresponding right cerebellar lesion (Figure 17). The pathological diagnosis was haemangioblastoma.

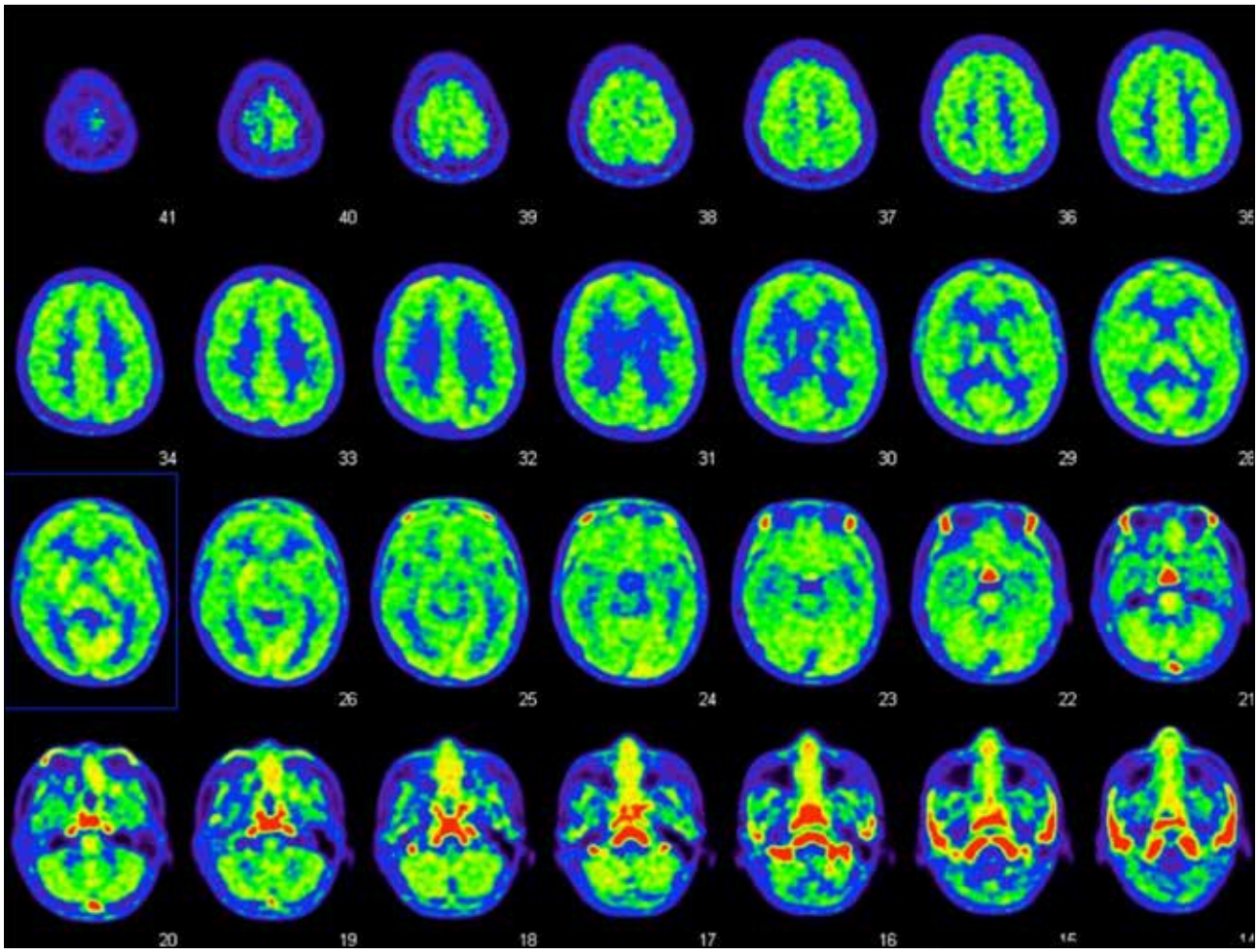

Figure 7. Basal ganglia germ cell tumour of the same patient in Figure 4. There is no residual ^{11}C-methionine tracer activity in the right basal ganglia and the thalamus, compared with pre-treatment positron emission tomography in Figure 6.

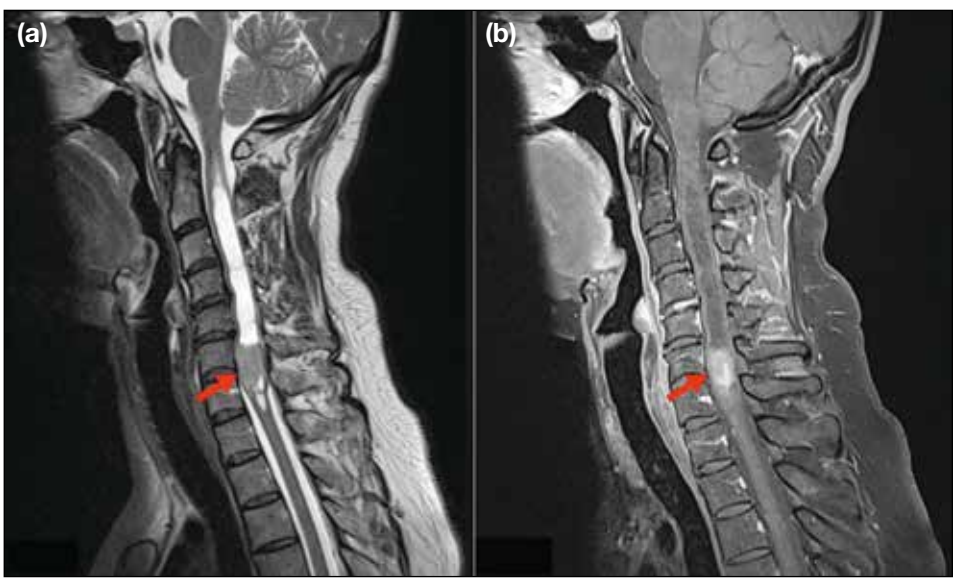

Figure 8. Grade 2 ependymoma of a 50-year-old patient. (a) Syringohydromyelia with an inferiorly located soft tissue nodule at the C6 to C7 vertebrae is seen on T2-weighted magnetic resonance imaging (MRI) [arrow]. (b) Enhancement of the soft tissue nodule is noted on post-gadolinium T1-weighted MRI (arrow).

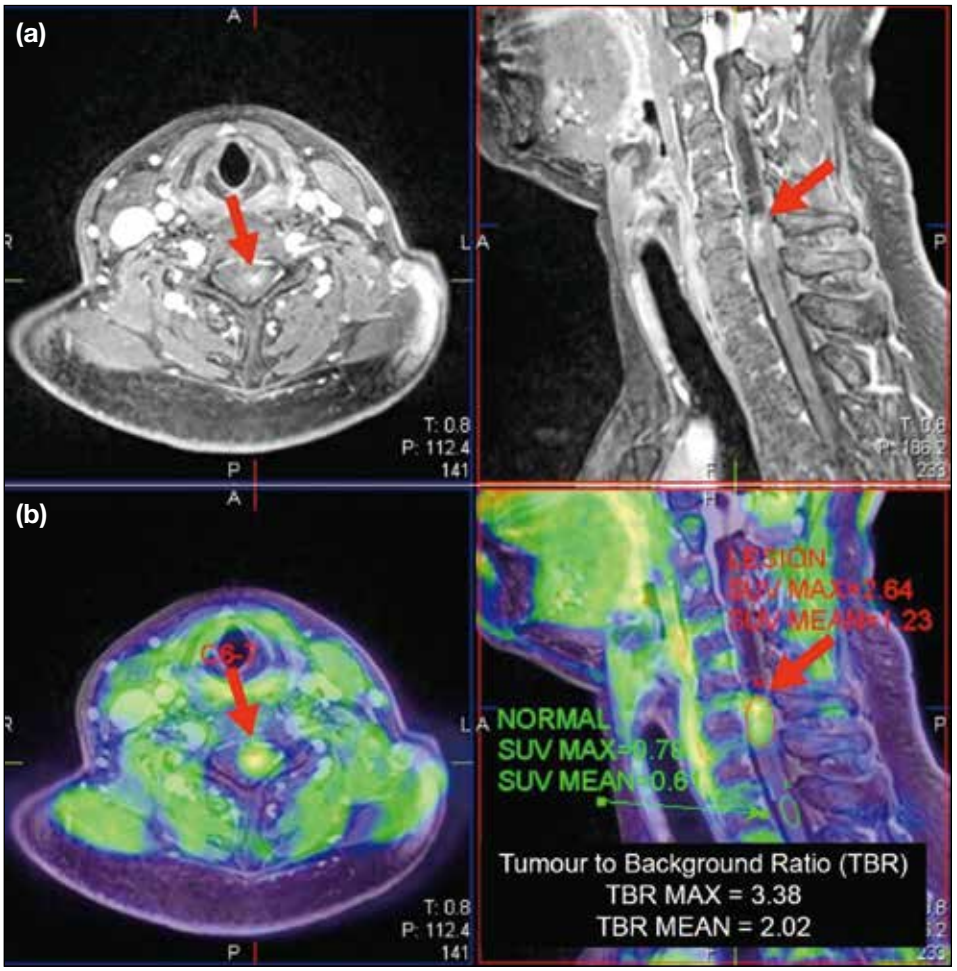

Figure 9. Grade 2 ependymoma of the same patient in Figure 8. (a) Enhancing soft tissue nodule at the C6 to C7 vertebrae (arrows) is seen on post-gadolinium T1-weighted magnetic resonance imaging (MRI) [upper row]. (b) Increased ^{18}F-fluoroethyl-L-tyrosine (^{18}F-FET) tracer uptake of the enhancing soft tissue nodule is noted on FET/MRI (lower row) [arrows]. There is no tracer activity along the wall of the syrinx. Images on the left show axial view while those on the right show sagittal view.
Abbreviations: SUV MAX = maximum standardised uptake value; SUV MEAN = mean standardised uptake value; TBR MAX = maximum tumour-to-background ratio; TBR MEAN = mean tumour-to-background ratio.

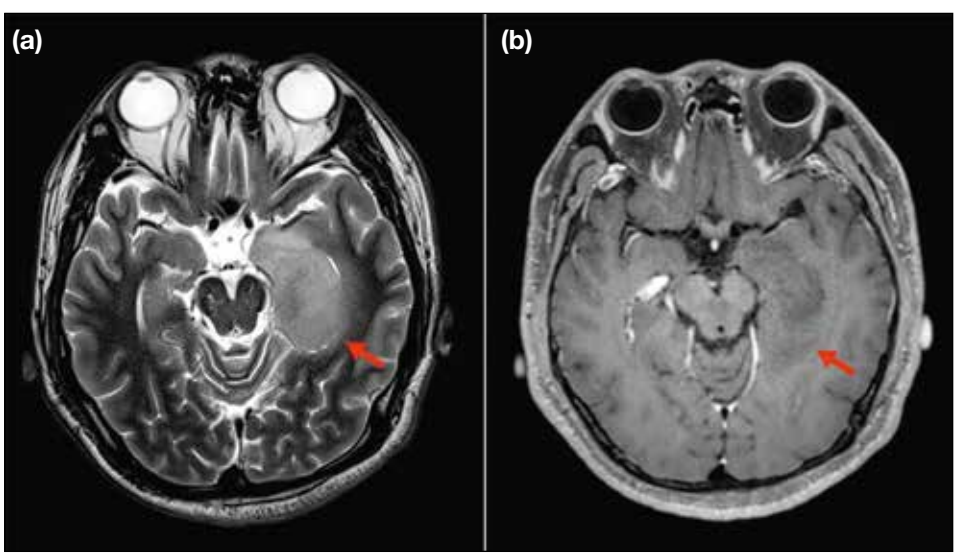

Figure 10. Glioblastoma of a 38-year-old patient. (a) Left temporal lobe infiltrative hyperintense lesion is seen on T2-weighted magnetic resonance imaging (MRI) [arrow]. (b) There is no enhancement on post-gadolinium T1-weighted MRI (arrow).

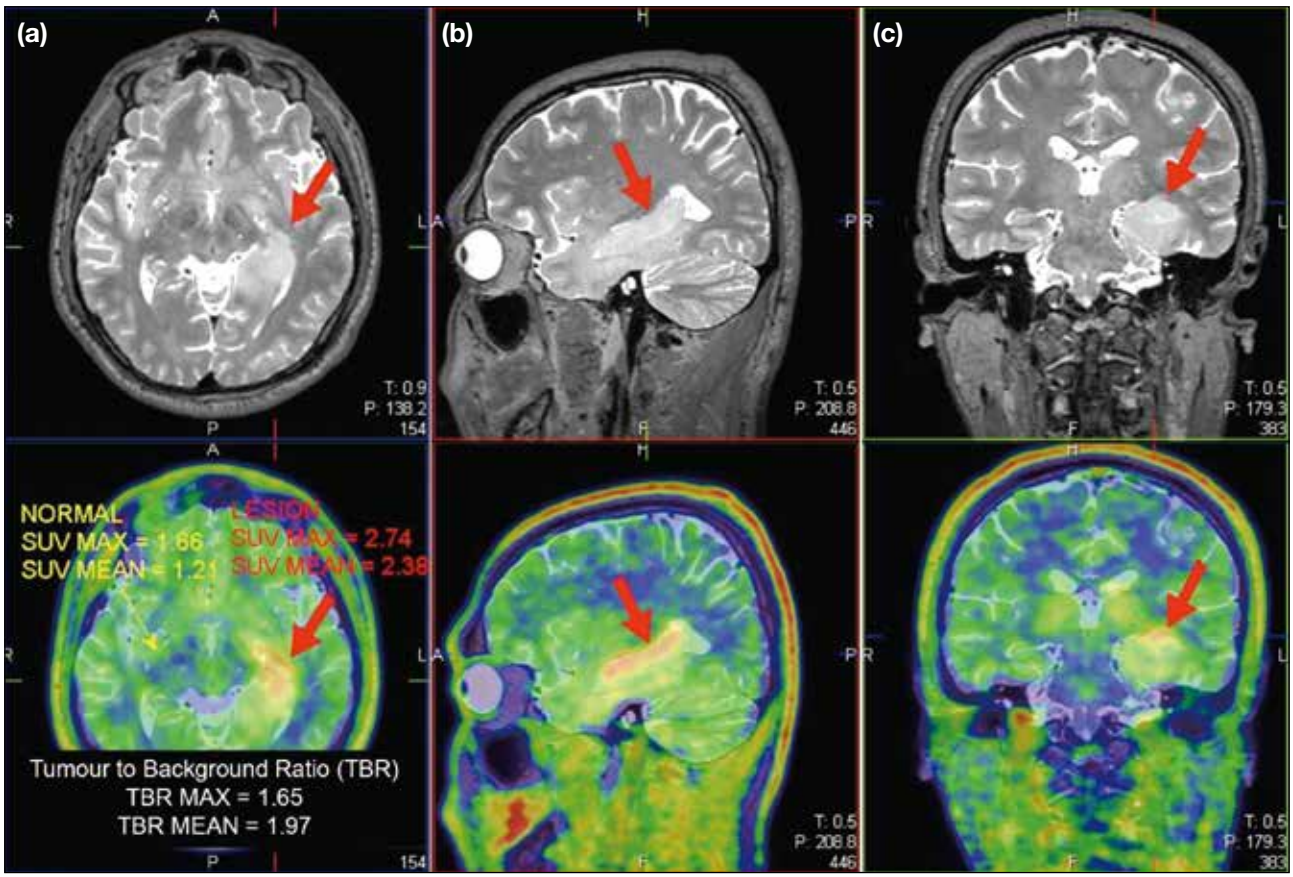

Figure 11. Glioblastoma, isocitrate dehydrogenase–wild type and telomerase reverse transcriptase mutation of the same patient in Figure 10. Images in the upper row are T2-weighted magnetic resonance imaging. There is increased ^{18}F-fluoroethyl-L-tyrosine tracer uptake in the left temporal lobe (arrows) on positron emission tomography–magnetic resonance imaging with a mean tumour-to-background ratio above imaging thresholds (lower row). (a) Axial view. (b) Sagittal view. (c) Coronal view.
Abbreviations: SUV MAX = maximum standardised uptake value; SUV MEAN = mean standardised uptake value; TBR MAX = maximum tumour-to-background ratio; TBR MEAN = mean tumour-to-background ratio.

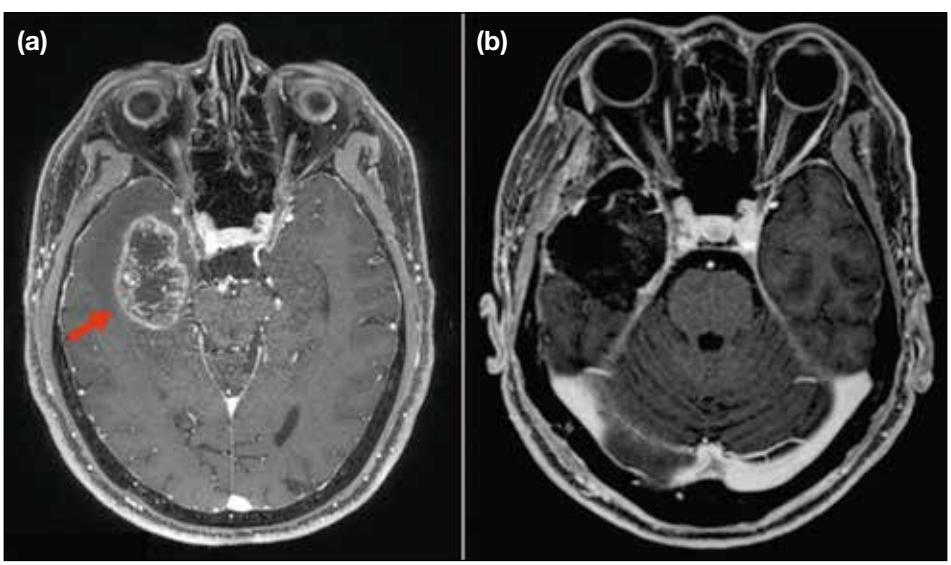

Figure 12. (a) Right anterior temporal lobe necrotic glioblastoma of a 63-year-old patient on post-gadolinium T1-weighted magnetic resonance imaging (MRI) before treatment (arrow). (b) Complete tumour removal on postoperative MRI.

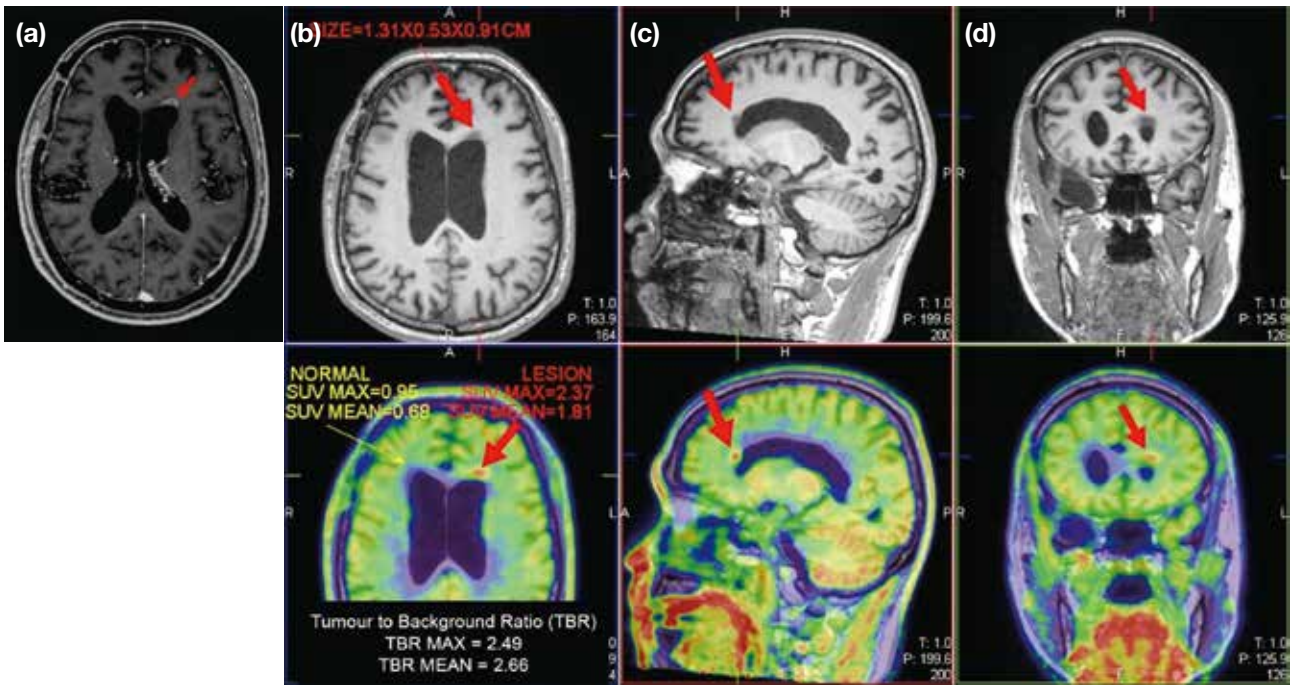

Figure 13. Recurrent glioblastoma of the same patient in Figure 12. (a) New enhancing nodule is seen in the left frontal lobe subependymal region on post-gadolinium T1-weighted magnetic resonance imaging (MRI) [arrow]. (b-d) Images in the upper row are T1-weighted magnetic resonance imaging. There is increased ^{11}C-methionine tracer uptake within the enhancing lesion (arrows) on positron emission tomography–magnetic resonance imaging (lower row). (b) Axial view. (c) Sagittal view. (d) Coronal view.
Abbreviations: SUV MAX = maximum standardised uptake value; SUV MEAN = mean standardised uptake value; TBR MAX = maximum tumour-to-background ratio; TBR MEAN = mean tumour-to-background ratio.

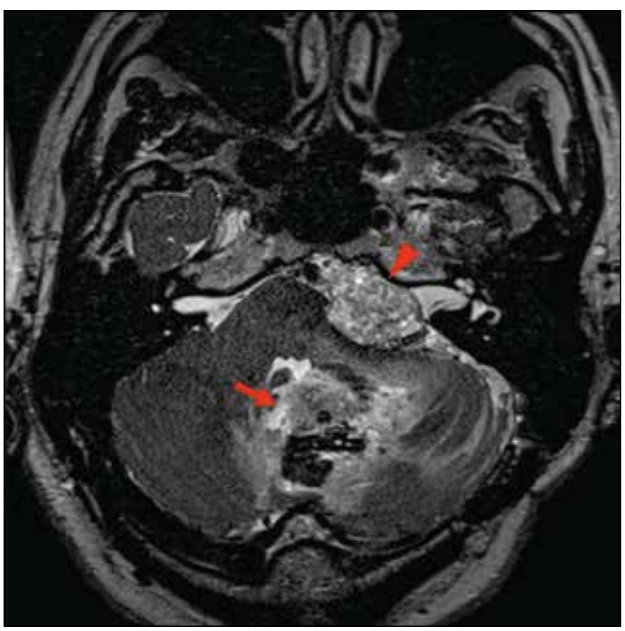

Figure 14. A 53-year-old patient with a history of left cerebellopontine angle (CPA) meningioma treated with resection and radiotherapy. Residual left CPA meningioma with postoperative and post-irradiation changes (arrowhead) are seen on follow-up T2-weighted magnetic resonance imaging. There is a new lesion in the left cerebellum with internal haemorrhage (arrow).

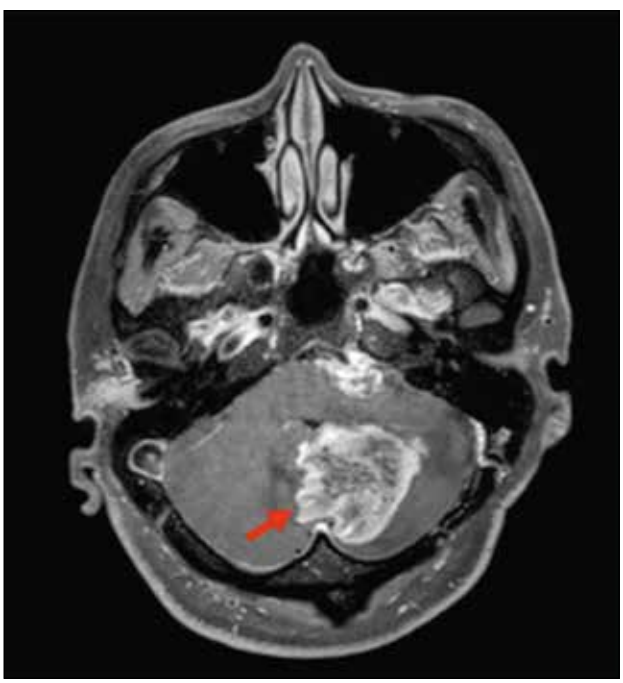

Figure 15. Glioblastoma of the same patient in Figure 14. Post-gadolinium T1-weighted magnetic resonance imaging shows a rim-enhancing lesion in the left cerebellum with central necrotic area (arrow).

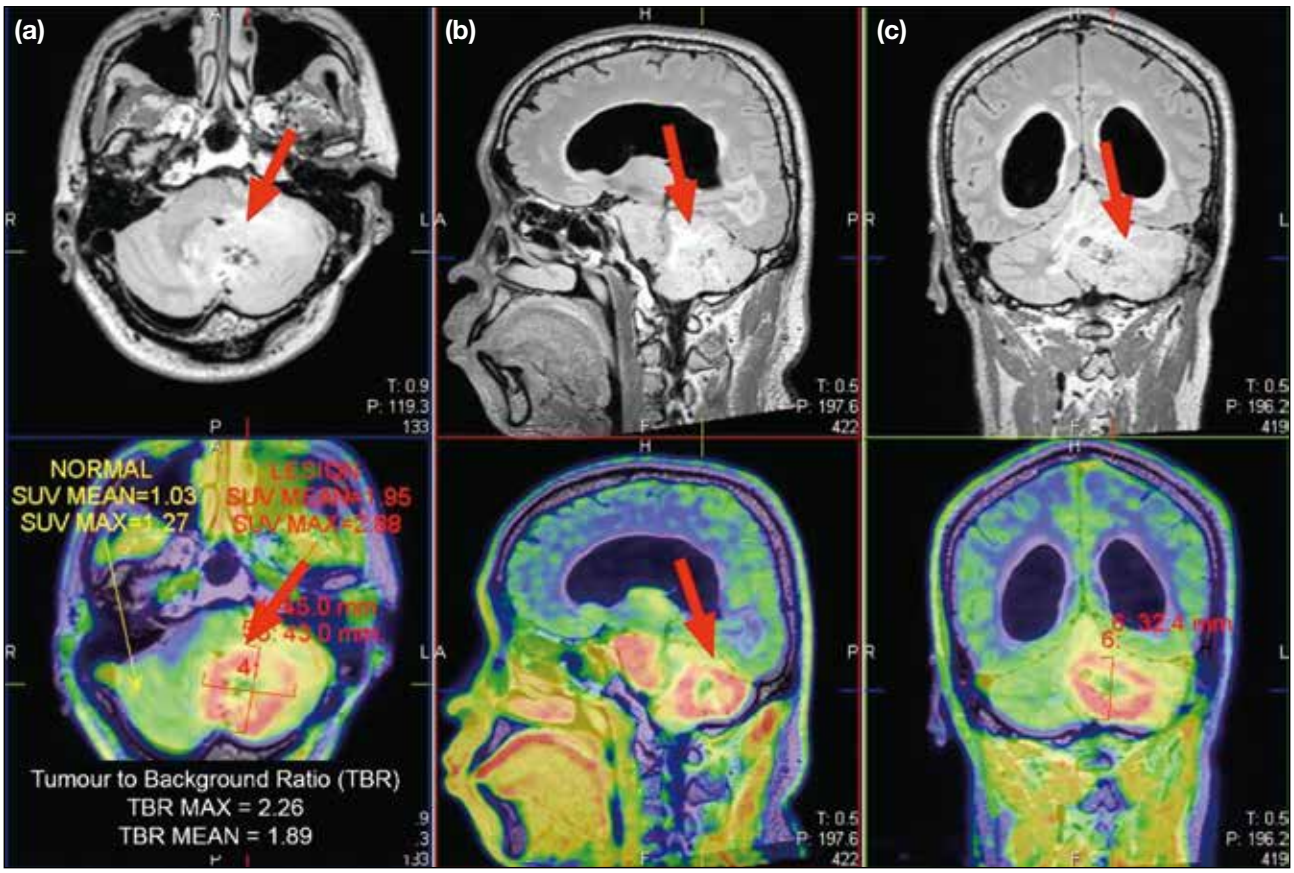

Figure 16. Glioblastoma of the same patient in Figure 14. Images in the upper row are T2-weighted fluid-attenuated inversion recovery magnetic resonance imaging. Positron emission tomography–magnetic resonance imaging shows increased ^{18}F-fluoroethyl-L-tyrosine uptake along the enhancing wall of the left cerebellar lesion (lower row) [arrows], with increased maximum and mean tumour-to-background ratios. (a) Axial view. (b) Sagittal view. (c) Coronal view.
Abbreviations: SUV MAX = maximum standardised uptake value; SUV MEAN = mean standardised uptake value; TBR MAX = maximum tumour-to-background ratio; TBR MEAN = mean tumour-to-background ratio.

CONCLUSION

AA-PET has been developed for decades yet not routinely implemented in neuro-oncology. Previously, PET was criticised for its poor spatial resolution. With technological advancement, the fusion of MRI and PET images can yield additional insight beyond either examination alone by differentiating neoplastic from non-neoplastic processes, preoperatively predicting the tumour grading according to the recommended cutoff values, as well as differentiating post-treatment changes from early tumour recurrence. The location within the tumour with the highest metabolic activity can be depicted to aid biopsy and operation. Hybrid PET/MRI is more patient-friendly and offers practical advantages; however, careful interpretation and post-processing of the images by experienced operators are crucial for the accuracy and reliability of the results. Further studies are needed to evaluate the role of AA-PET, with the emerging classification of central nervous system tumours, in predicting IDH status and other radiogenomic applications in precision cancer medicine.

REFERENCES

1. Law I, Albert NL, Arbizu J, Boellaard R, Drzezga A, Galldiks N, et al. Joint EANM/EANO/RANO practice guidelines/SNMMI procedure standards for imaging of gliomas using PET with radiolabelled amino acids and [^{18}F]FDG: version 1.0. Eur J Nucl Med Mol Imaging. 2019;46:540-57.
2. Kracht LW, Miletic H, Busch S, Jacobs AH, Voges J, Hoevels M, et al. Delineation of brain tumor extent with [^{11}C]L-methionine positron emission tomography: local comparison with stereotactic histopathology. Clin Cancer Res. 2004;10:7163-70.
3. Pauleit D, Floeth F, Hamacher K, Riemenschneider MJ, Reifenberger G, Müller HW, et al. *O*-(2-[^{18}F]fluoroethyl)-L-tyrosine PET combined with MRI improves the diagnostic assessment of cerebral gliomas. Brain. 2005;128:678-87.

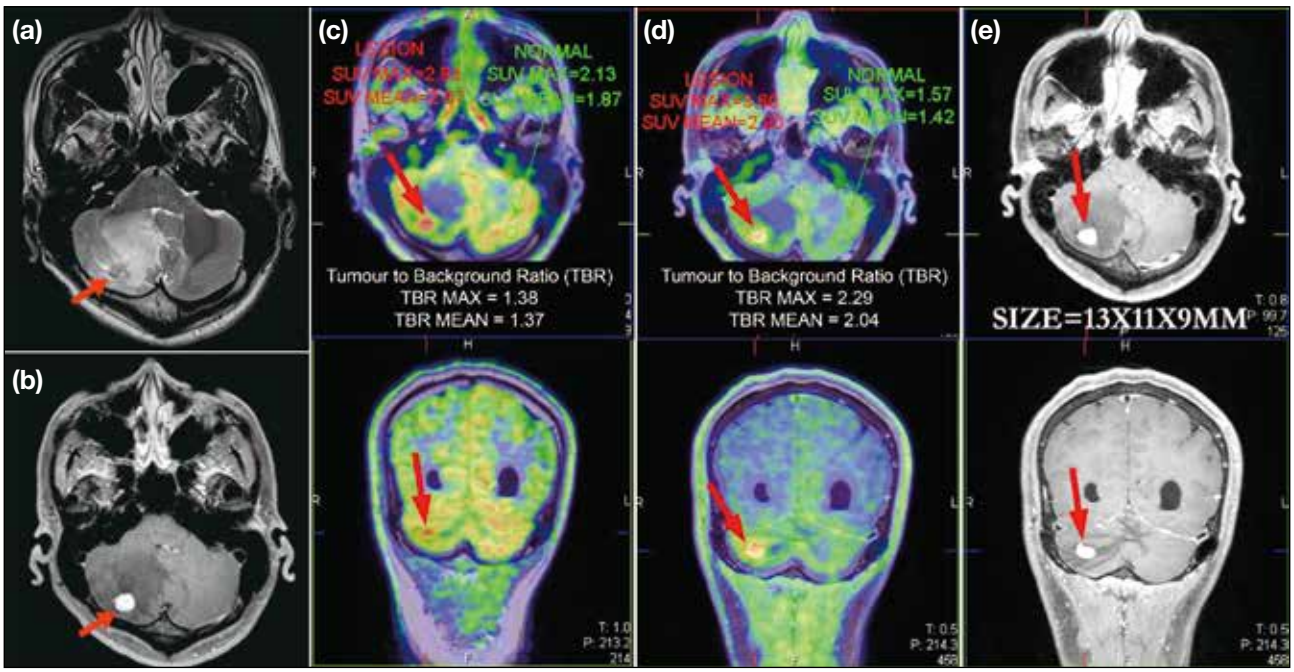

Figure 17. Haemangioblastoma of a 45-year-old patient. (a) Heterogeneous T2-weighted hyperintense cortical locating right cerebellar lesion (arrow) with perifocal vasogenic oedema. (b) Intense solid enhancement without cystic component is seen on post-gadolinium T1-weighted magnetic resonance imaging (arrow). Strong nodular ^{11}C-methionine (c) and ^{18}F-fluoroethyl-L-tyrosine (d) tracer uptake (arrows) on positron emission tomography–magnetic resonance imaging of the lesion was pathology-proven haemangioblastoma. (e) Post-gadolinium T1-wighted magnetic resonance imaging of the brain. (c-e) Axial view (upper row) and coronal view (lower row).
Abbreviations: SUV MAX = maximum standardised uptake value; SUV MEAN = mean standardised uptake value; TBR MAX = maximum tumour-to-background ratio; TBR MEAN = mean tumour-to-background ratio.

4. Rapp M, Heinzel A, Galldiks N, Stoffels G, Felsberg J, Ewelt C, et al. Diagnostic performance of ^{18}F-FET PET in newly diagnosed cerebral lesions suggestive of glioma. J Nucl Med. 2013;54:229-35.
5. Herholz K, Hölzer T, Bauer B, Schröder R, Voges J, Ernestus RI, et al. ^{11}C-methionine PET for differential diagnosis of low-grade gliomas. Neurology. 1998;50:1316-22.
6. Kunz M, Thon N, Eigenbrod S, Hartmann C, Egensperger R, Herms J, et al. Hot spots in dynamic ^{18}FET-PET delineate malignant tumor parts within suspected WHO grade II gliomas. Neuro Oncol. 2011;13:307-16.
7. Pirotte BJ, Levivier M, Goldman S, Massager N, Wikler D, Dewitte O, et al. Positron emission tomography–guided volumetric resection of supratentorial high-grade gliomas: a survival analysis in 66 consecutive patients. Neurosurgery. 2009;64:471-81; discussion 481.
8. Pöpperl G, Kreth FW, Mehrkens JH, Herms J, Seelos K, Koch W, et al. FET PET for the evaluation of untreated gliomas: correlation of FET uptake and uptake kinetics with tumour grading. Eur J Nucl Med Mol Imaging. 2007;34:1933-42.
9. WHO Classification of Tumours Editorial Board. WHO Classification of Tumours, 5th Edition, Volume 6: Central Nervous System Tumours. World Health Organization: 2021.
10. Vettermann F, Suchorska B, Unterrainer M, Nelwan D, Forbrig R, Ruf V, et al. Non-invasive prediction of IDH-wildtype genotype in gliomas using dynamic ^{18}F-FET PET. Eur J Nucl Med Mol Imaging. 2019;46:2581-9.
11. Verger A, Stoffels G, Bauer EK, Lohmann P, Blau T, Fink GR, et al. Static and dynamic ^{18}F-FET PET for the characterization of gliomas defined by IDH and 1p/19q status. Eur J Nucl Med Mol Imaging. 2018;45:443-51.
12. Rottenburger C, Doostkam S, Prinz M, Meckel S, Nikkhah G, Meyer PT, et al. Interesting image. Amino acid PET tracer accumulation in cortical ischemia: an interesting case. Clin Nucl Med. 2010;35:907-8.
13. Pichler R, Wurm G, Nussbaumer K, Kalev O, Silye R, Weis S. Sarcoidois and radiation-induced astrogliosis causes pitfalls in neuro-oncologic positron emission tomography imaging by *O*-(2-[^{18}F]fluoroethyl)-L-tyrosine. J Clin Oncol. 2010;28:e753-5.
14. Salber D, Stoffels G, Oros-Peusquens AM, Shah NJ, Reifenberger G, Hamacher K, et al. Comparison of *O*-(2-^{18}F-fluoroethyl)-L-tyrosine and L-^{3}H-methionine uptake in cerebral hematomas. J Nucl Med. 2010;51:790-7.
15. Salber D, Stoffels G, Pauleit D, Oros-Peusquens AM, Shah NJ, Klauth P, et al. Differential uptake of *O*-(2-^{18}F-fluoroethyl)-L-tyrosine, L-^{3}H-methionine, and ^{3}H-deoxyglucose in brain abscesses. J Nucl Med. 2007;48:2056-62.
16. Stockhammer F, Prall F, Dunkelmann S, Plotkin M, Piek J. Stereotactic biopsy of a cerebral capillary telangiectasia after a misleading F-^{18}-FET-PET. J Neurol Surg A Cent Eur Neurosurg. 2012;73:407-9.